Dielectronic recombination of Rh-like Gd and W

B. W. Li and G. O'Sullivan
School of Physics, University College Dublin, Belfield, Dublin 4, Ireland

Y. B. Fu and C. Z. Dong
Key Laboratory of Atomic and Molecular Physics & Functional Materials of Gansu Province, College of Physics and Electronics Engineering, orthwest Normal University, Lanzhou 730070, China, and Joint Laboratory of Atomic and Molecular Physics, NWNU & IMP CAS, Lanzhou 730070, China

(Received 17 April 2012; published 15 May 2012)

Ab initio calculations of dielectronic recombination rate coefficients of Rh-like gadolinium and tungsten have been performed. Energy levels, radiative transition probabilities, and autoionization rates of Pd-like gadolinium and tungsten for [Zn]$4p^6 4d^8 4fnl$, [Zn]$4p^6 4d^8 5l'nl$, [Zn]$4p^6 4d^8 6l'nl$ and [Zn]$4p^5 4d^{10} nl$, [Zn]$4p^5 4d^9 4fnl$, [Zn]$4p^5 4d^9 5l'nl$, [Zn]$4p^5 4d^9 6l'nl$ ($n \leqslant 18$) complexes were calculated using the flexible atomic code. The contributions from resonant and nonresonant radiative stabilizing transitions to the total rate coefficients are discussed. Results show that the contributions from nonresonant radiative stabilizing transitions are significantly enchanced for W when compared with Gd as a result of lowering of energy levels relative to the ionization limit. In addition, the widely used Burgess-Merts semiempirical formula may underestimate the dielectronic recombination rate coefficients in the temperature regions of interest. The present calculated rate coefficients are fitted to a semiemperical formula. The data obtained are expected to be useful for modelling plasmas both for extreme ultraviolet lithography source development and for fusion applications.

DOI: 10.1103/PhysRevA.85.052706 PACS number(s): 34.80.Lx

I. INTRODUCTION

The dielectronic recombination (DR) process plays an important role in high-temperature plasmas, where it affects both the ionization balance and radiative energy losses. Plasmas containing gadolinium have been proposed as sources for next-generation extreme ultraviolet lithography (EUVL) near 6.7 nm. Reliable atomic data including energy levels, transition probabilites, and rate coefficients for various dynamic processes are urgently needed. In the past, the DR rate of Ni-like gadolinium, where the DR process can provide a potential source for soft x-ray laser operation, has been studied [1–3]. Tungsten is being considered as a plasma-facing material in magnetically confined fusion devices, such as ITER, because of its low sputtering rate, high-temperature characteristics, and low tritium absorption. Considerable effort has been made to obtain reliable atomic data to enable identification of reference lines for plasma diagnostics and to reliably estimate radiative cooling rates (see most recently review papers [4–8]). In contrast to the situation for Gd, a significant number of publications on DR processes have been published for tungsten [9–24]. In all reported studies of gadolinium and tungsten plasmas, their emission is dominated by Ag- and Pd-like lines, that is, the spectra resulting from ions with either a closed outermost subshell (Pd-like) or a configuration with a single electron outside a closed subshell (Ag-like), where the emission is not spread among many transitions [23–28]. Recently, Safronova and co-workers studied the DR rate coefficients for Pd-like W [20]. Li and co-workers studied the DR rate coefficients for Pd-like Gd and found that DR is a very important recombination mechanism for Pd-like Gd in EUVL source plasmas and one that can enhance the population of Ag-like ions [29]. However, due to the complexity of the calculations as open $4d$ and $4f$ shells are involved, very few *ab initio* level-by-level DR calculations are available for Rh-like Gd and W and the rates for these are important as they contribute to the population of Pd-like ions.

In this paper, we report on the detailed calculation of DR rate coefficients for Rh-like gadolinium and tungsten. The relativistic flexible atomic code (FAC) [30] was used to calculate the atomic structure, radiative transition probablities, and autoionization probablities. In Sec. II, we briefly outline the theoretical methods used for the calculation of DR rate coefficients. The DR rate coefficients obtained are presented and discussed in Sec. III.

II. THEORETICAL METHOD

The DR process can be described as the resonant capture of an incident electron by an ion, followed by radiative decay which competes with autoionization (AI). The first step is the resonant capture process in which a free electron is captured by an ion while a bound electron is excited. The capture-excitation process can be schematically written as follows:

$$\begin{aligned}[\mathrm{Zn}]\,4p^6 4d^9 + e &\rightarrow [\mathrm{Zn}]\,4p^6 4d^8 n'l'nl,\ n'l' \\ &= 4f,\ 5l,\ 6l,\ +\ 4p^5 4d^{10} nl + 4p^5 4d^9 n'l'nl,\ n'l' \\ &= 4f,\ 5l,\ 6l. \end{aligned} \tag{1}$$

It is the inverse process of AI, sometimes called dielectronic capture (DC).

The second step in the DR process is autoionizing state decay by emission of either an Auger electron or a photon into a lower state. It can be schematically written as follows:

$$\begin{aligned}&[\mathrm{Zn}]\ 4p^6 4d^8 n'l'nl + 4p^5 4d^{10} nl + 4p^5 4d^9 n'l'nl, \\ &\quad\rightarrow [\mathrm{Zn}]\ 4p^6 4d^9\ nl + 4p^6 4d^8\ n'l'n''l'' + h\nu, \end{aligned} \tag{2}$$

$$\downarrow$$

$$[\mathrm{Zn}]\ 4p^6 4d^9 + e \tag{3}$$

The first term in Eq. (2) represents the decay from AI states to singly excited states, known as resonant stabilizing transitions (RS). The second term represents the decays to doubly excited states which are below the ionization limit, known as nonresonant stabilizing (NRS) transitions. Another possible decay is to lower states that still lie above the ionization limit and then further decay by either AI or radiative decay cascade (DAC) transitions. However, as research results show, the DR rates are less affected by DAC for the heavy elements and thus can be neglected for most applications [31]. Disregarding DAC then leads to the following approximation for the DR branching ratio [31]:

$$B_j^r = \frac{\sum_f A_{jf}^r + \sum_{f'} A_{jf'}^r}{\sum_{i'} A_{di'}^a + \sum_f A_{jf}^r + \sum_{f'} A_{jf'}^r}. \tag{4}$$

Here A^a and A^r are the Auger and radiative rates, respectively. f denotes singly excited final states, f' denotes doubly excited final states that lie below the ionization limit, d denotes doubly excited final states lying above the ionization threshold, and i' is the final state of the Auger decay.

In the isolated resonance approximation, assuming that the electron velocity distribution in the plasma is Maxwellian, the DR rate coefficients can be expressed as

$$\alpha_{\mathrm{i}}^{DR}(T_e) = \frac{h^3}{(2\pi m_e T_e)^{3/2}} \sum_j \frac{Q_j}{2g_i} \exp\left(-\frac{E_{ij}}{kT_e}\right), \tag{5}$$

where Q_j is the so-called intensity factor, defined as

$$Q_j = g_j A_{ji}^a B_j^r, \tag{6}$$

g_j and g_i are the statistical weights of the doubly excited AI state j and initial state i, respectively, and E_{ij} is resonant energy.

The contributions from higher-n states may be extrapolated up to $n = 1000$ using empirical scaling formulae (see Ref. [19] for details).

III. RESULTS AND DISCUSSION

In the present work, we report the results of detailed level-by-level calculations of the rate coefficients for DR through the following Rh-like Gd and W autoionizing inner-shell excited configuration complexes: $4d^8 4fnl$, $4d^8 5l'nl$, $4d^8 6l'nl$ and $4p^5 4d^{10} nl$, $4p^5 4d^9 4fnl$, $4p^5 4d^9 5l'nl$, $4p^5 4d^9 5l'nl$, ($n \leqslant 18$, $l \leqslant 5$). These resonant configurations are associated with $\Delta n = 0$, $\Delta n = 1$, and $\Delta n = 2$ core excitations of the $4d$ and $4p$ subshells, respectively. As previous research has shown that complexes resulting from $4p$ core excitation significantly influence the total DR rate coefficient [29], we explicitly include here the contributions from these complexes also. Energy levels, radiative transition probabilities, and AI rates are calculated using FAC.

A. Energy levels

The energy levels near the ionization limits for $4d$ and $4p$ subshell excitation are presented in Figs. 1 and 2, respectively. It should be noted that not all the above-listed doubly excited states can autoionize. Therefore, autoionizing intermediate states can be stabilized to these levels through NRS transitions. For Gd, as one can see from Fig. 2, the doubly excited $4d^8 4f^2$, $4d^8 4f5l$ ($l \leqslant 4$), $4d^8 4f6l$ ($l \leqslant 1$), $4d^8 5s5l$ ($l \leqslant 3$), $4d^8 5s6l$ ($l \leqslant 1$), $4d^8 5p5l$ ($l \leqslant 2$) resulting from $4d$ subshell excitation and $4p^5 4d^{10} 4f$, $4p^5 4d^{10} 5l$ ($l \leqslant 4$), $4p^5 4d^{10} 6l$ ($l \leqslant 2$), $4p^5 4d^9 4f^2$, $4p^5 4d^9 4f5s$, $4p^5 4d^9 5s^2$ which arise from $4p$ subshell excitation are below the ionization limit. For W, as Z increases, due to the lowering of these configurations as a result of increased binding, more levels lie below the ionization limit which results in closure of DR channels. Apart from the configurations just mentioned for Gd, $4d^8 4f6l$ ($l \leqslant 5$), $4d^8 4f7l$ ($l \leqslant 2$), $4d^8 5s5g$, $4d^8 5s6d$, $4d^8 5p5f$, $4d^8 5p6s$, $4d^8 5d^2$ due to $4d$ core excitation and $4p^5 4d^{10} 6l$ ($l \leqslant 5$), $4p^5 4d^{10} 7l$ ($l \leqslant 2$), $4p^5 4d^9 4f5l$ ($l \leqslant 3$), $4p^5 4d^9 5s5p$ from $4p$ core excitation lie below the ionization limit for W. As a result, the contribution of NRS will significantly increase for high-temperature plasmas of W when compared to Gd, as we show later. It should be mentioned that the present calculated ionization potential usd here for Pd-like W is

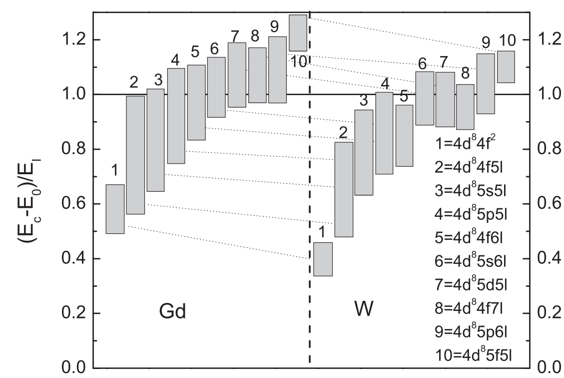

FIG. 1. Energy levels of doubly excited configurations within the $4d$ complexes relative to the first ionization limit E_I (565 eV for Gd and 1128 eV for W), which is indicated by the dashed line. E_0 is the gound-state energy of Pd-like Gd and W. The energies are indicated by a finite vertical range representing the full level spread within each configuration.

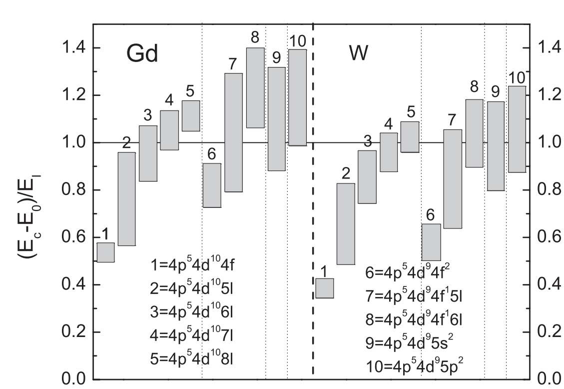

FIG. 2. Energy levels of doubly excited configurations within the $4p$ complexes relative to the first ionization limit E_I (565 eV for Gd and 1128 eV for W), which is indicated by the dashed line. E_0 is the gound-state energy of Pd-like Gd and W. The energies are indicated by a finite vertical range representing the full level spread within each configuration.

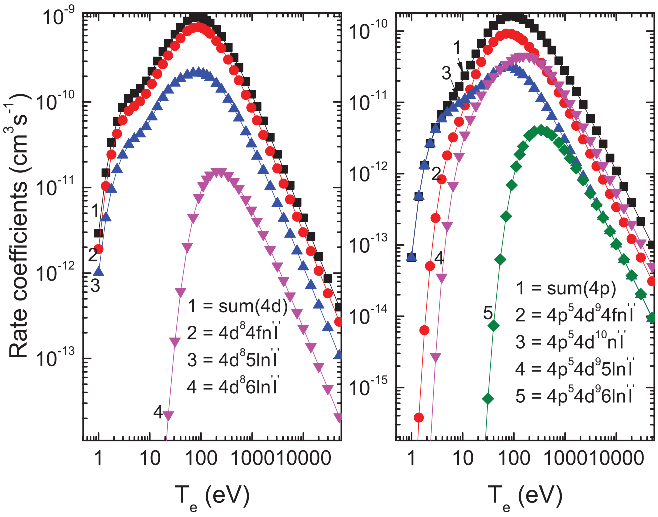

FIG. 3. (Color online) Partial DR rate coefficients for $4d$ and $4p$ core excited complexes of Gd.

1128 eV, which compares well with the value of 1132 eV calculated by Kramida and Reader [32].

B. The partial DR rate coefficients

The partial DR rate coefficients of different complexes for Gd and W are presented in Figs. 3 and 4, respectively. Take Gd as an example. For $4d$ subshell excitations, the contribution from 4d^{8}4fnl complexes to the total DR rate is more than 70% at temperatures below 1 keV. The relative contribution from $4d^85l'nl$ complexes is about 23% near 110 eV. The influence of $4d^86l'nl$ complexes is less than 6%. This means that for $4d$ subshell excitation, $\Delta n = 0$ core excitation makes the dominant contribution should always be included in calculations for other $4d$ open shell ions. For $4p$ subshell excitation, the contribution from the resulting complexes to the total DR rate coefficients is less than 25% when compared with $4d$ subshell excitation. The contribution from $4p^54d^94fnl$ complexes is, however, greater than 50% in the

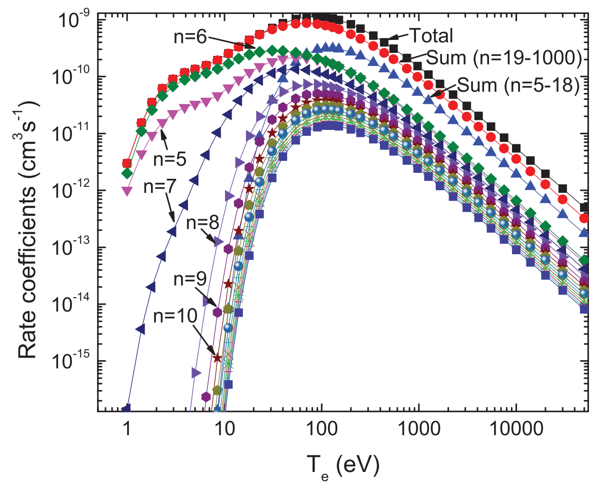

FIG. 5. (Color online) The DR rate coefficients where an incident electron is captured to the different orbitals of Gd.

20- to 150-eV region. The $4p^54d^95l'nl$ contribution overtakes that from $4p^54d^94fnl$ complexes when the temperature exceeds 440 eV. The contribution from $\Delta n = 2$ $4p$ core excitations is everywhere less than 10%.

In addition, our previous studies on Pd-like Gd showed that the contributions from $4s$ subshell excitations to the overall DR coefficient is almost two orders of magnitude lower than the total DR rate coefficients throughout the whole temperature region covered in the above figures. Moreover, from other studies it can be inferred that the influence of $3d$-core excitation is much smaller than for the $4s$ shell [33]. Therefore, the contributions from $4s$ and $3d$ complexes can be essentially ignored in the present calculations.

C. The total DR rate coefficients

Figures 5 and 6 show the contributions of DR rate coefficients where a free electron is captured to different n shells for Gd and W. For Gd, $n = 6$ provides the most important capture channel at temperatures below 100 eV. The DR rate coefficients change regularly when $n > 7$. However,

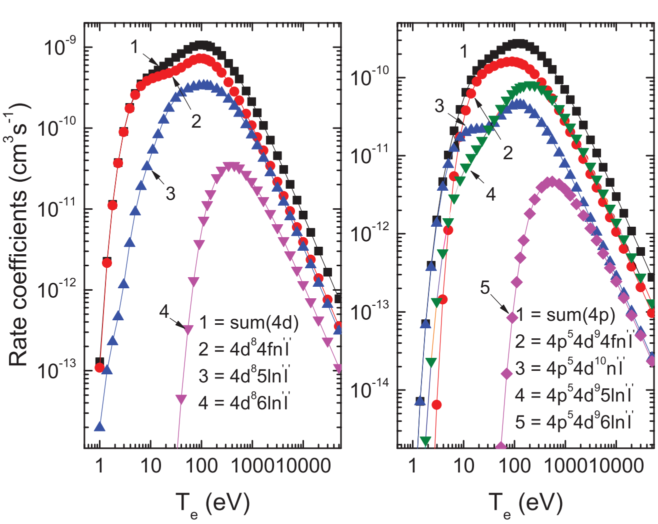

FIG. 4. (Color online) Partial DR rate coefficients for $4d$ and $4p$ core excited complexes of W.

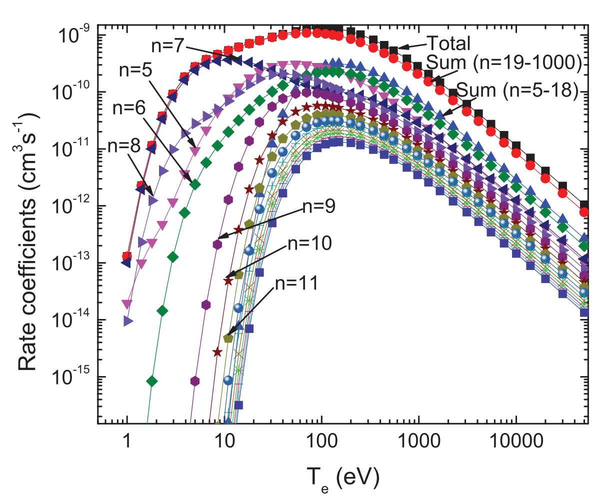

FIG. 6. (Color online) The DR rate coefficients where an incident electron is captured to the different orbitals of W.

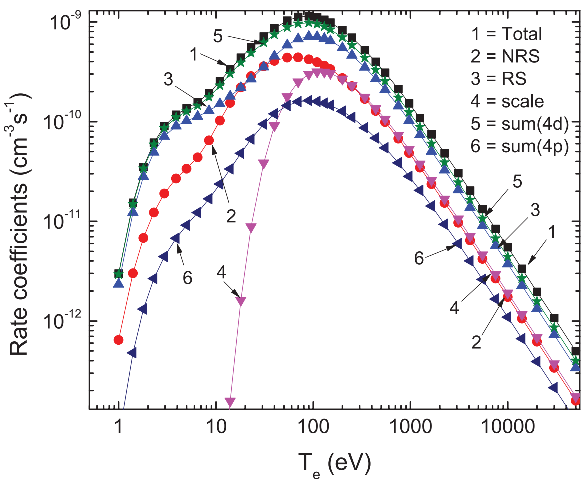

FIG. 7. (Color online) Contributions from the RS and NRS transition as well as different core excitations to total DR rate coefficients as a function of T_e in Rh-like Gd.

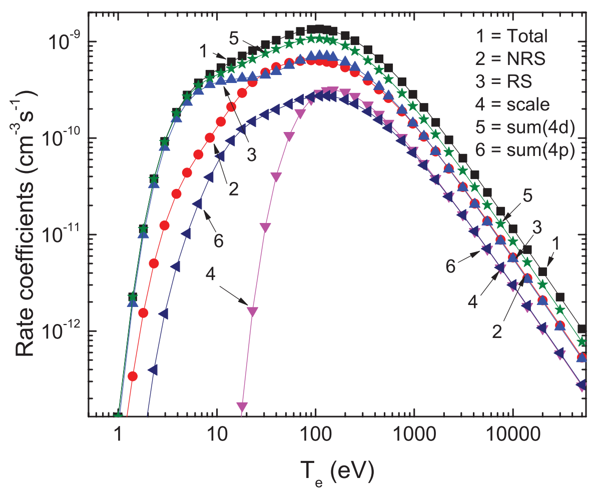

FIG. 8. (Color online) Contributions from the RS and NRS transition as well as different core excitations to total DR rate coefficients as a function of T_e in Rh-like W.

the n dependence for W is much more complicated for states with $n < 9$ at lower temperatures. This behavior arises mainly because of the influence of near-threshold states, especially for those configurations that are partially autoionizing, since their resonant energies are quite small but the DR rate coefficients have an $\exp(-E_{ij}/kT_e)$ dependance. Small changes in the relative position of the ionization limit may result in closure of some channels thus impacting on the DR rates. The $4d^85p5f$ $(n = 5)$ and $4d^84f6d$ $(n = 6)$ configurations for Gd, and the $4d^85p5g$ and $4d^85d5f$ $(n = 5)$, $4d^85s6f$ $(n = 6)$, $4d^84f7f$ and $4d^84f7g$ $(n = 7)$, $4d^84f8s$ $(n = 8)$ for W give the biggest contribution at temperatures lower than 15 eV. However, as the temperature increases, their influence is less important.

The resulting total DR rate coefficients are plotted together with the partial rates for RS and NRS transitions in Figs. 7 and 8 for Gd and W. The $4d$ subshell makes the biggest contribution for both ions. An interesting change that should be noted arises from the influence of NRS transitions. The RS rate coefficient exceeds that for NRS at both lower and higher temperatures and is nearly the same around 15–40 eV for Gd. However, this is different for W, where the NRS decay rate is comparable with that for RS when the temperature is higher than 25 eV. As before, the presence of more doubly excited states below the ionization limit as Z increases results in more NRS decay channels.

A widely used semiempirical formula was given by Burgess [34] and modified by Merts *et al.* [35], which is known as the Burgess-Merts (BM) approximation. The BM approximation is, in principle, suitable for ionization stages <20 (although this approximation is still used for other ionic stages since no universal formula exists). We compare the

TABLE I. Fitting coefficients using Eq. (7) for Rh-like Gd. $A[B]$ denote $A \times 10^B$.

n	c_1	E_1	c_2	E_2	c_3	E_3	c_4	E_4	c_5	E_5
$n = 5$–1000	6.580[–9]	7.856[0]	8.007[–8]	3.174[1]	1.437[–6]	3.324[2]	5.286[–7]	6.411[1]	3.519[–6]	1.564[2]
$n = 5$–18	6.462[–8]	3.028[1]	6.488[–9]	7.824[0]	4.827[–7]	6.072[1]	1.893[–6]	1.423[2]	1.177[–6]	3.211[2]
$n = 19$–1000	1.702[–6]	1.720[2]	2.433[–7]	3.765[2]						
$n = 5$	2.775[–7]	1.795[2]	2.204[–7]	1.018[2]	9.760[–8]	4.825[1]	1.198[–9]	7.163[0]	1.972[–9]	1.635[1]
$n = 6$	2.286[–8]	2.631[1]	1.703[–7]	5.088[1]	2.506[–7]	2.710[2]	2.125[–7]	1.350[2]	4.838[–9]	7.838[0]
$n = 7$	2.611[–8]	4.161[1]	1.122[–7]	1.841[2]	1.523[–7]	3.462[2]	1.670[–7]	8.064[1]	4.088[–10]	1.830[1]
$n = 8$	8.023[–8]	1.168[2]	2.262[–8]	7.778[1]	9.335[–8]	2.467[2]	7.284[–8]	1.007[2]	8.000[–8]	4.062[2]
$n = 9$	5.084[–8]	4.385[2]	4.736[–8]	1.335[2]	5.913[–8]	1.093[2]	7.357[–8]	2.784[2]	4.712[–8]	1.337[2]
$n = 10$	5.966[–8]	1.258[2]	2.604[–8]	1.638[2]	5.776[–8]	3.032[2]	5.315[–8]	1.399[2]	3.439[–8]	4.617[2]
$n = 11$	4.409[–8]	1.383[2]	4.500[–8]	3.146[2]	3.877[–8]	1.664[2]	4.189[–8]	1.395[2]	2.585[–8]	4.734[2]
$n = 12$	2.058[–8]	4.797[2]	3.572[–8]	3.215[2]	4.289[–8]	1.464[2]	3.326[–8]	1.728[2]	3.740[–8]	1.464[2]
$n = 13$	3.102[–8]	3.138[2]	–3.523[–9]	2.871[2]	1.844[–8]	4.762[2]	5.906[–8]	1.504[2]	4.436[–8]	1.695[2]
$n = 14$	3.719[–8]	1.591[2]	2.134[–8]	1.869[2]	2.374[–8]	3.376[2]	3.873[–8]	1.559[2]	1.229[–8]	4.953[2]
$n = 15$	5.907[–10]	3.336[2]	1.681[–10]	3.307[2]	1.628[–10]	3.337[2]				
$n = 16$	1.567[–8]	3.254[2]	1.048[–8]	4.851[2]	2.362[–8]	1.739[2]	3.591[–8]	1.595[2]	2.328[–8]	1.769[2]
$n = 17$	2.532[–8]	1.738[2]	8.900[–9]	4.863[2]	2.434[–8]	1.786[2]	1.323[–8]	3.267[2]	2.766[–8]	1.608[2]
$n = 18$	2.777[–8]	1.676[2]	1.774[–8]	1.920[2]	2.781[–8]	1.676[2]	1.185[–8]	3.479[2]	6.028[–9]	5.044[2]

TABLE II. Fitting coefficients using Eq. (7) for Rh-like W. $A[B]$ denote $A \times 10^B$.

n	c_1	E_1	c_2	E_2	c_3	E_3	c_4	E_4	c_5	E_5	c_6	E_6	c_7	E_7
$n = 5$–1000	8.485[–7]	8.489[2]	2.534[–7]	4.462[2]	3.435[–6]	3.515[2]	2.581[–8]	1.994[1]	2.516[–6]	6.626[2]	3.391[–8]	1.283[1]	4.644[–8]	1.948[2]
$n = 5$–18	6.408[–7]	6.481[2]	4.145[–8]	1.323[1]	9.229[–8]	3.141[1]	2.946[–6]	5.839[2]	3.225[–6]	2.805[2]	1.797[–6]	1.438[2]		
$n = 19$–1000	2.863[–7]	5.105[2]	1.110[–6]	2.231[2]	2.870[–7]	7.984[2]	1.329[–6]	2.158[2]						
$n = 5$	3.801[–7]	3.190[2]	2.460[–9]	1.792[1]	4.735[–7]	1.815[2]	2.841[–7]	7.034[1]	5.260[–8]	3.642[1]				
$n = 6$	6.330[–9]	2.742[1]	9.055[–7]	2.698[2]	4.283[–7]	1.480[2]	7.668[–7]	4.679[2]	1.024[–7]	6.877[1]				
$n = 7$	4.953[–7]	3.070[2]	1.015[–7]	1.674[2]	6.226[–7]	5.557[2]	1.276[–8]	1.455[1]	1.164[–8]	1.197[1]	1.611[–8]	1.450[1]	4.915[–8]	3.684[1]
$n = 8$	2.724[–7]	3.392[2]	1.026[–7]	6.859[1]	2.053[–8]	1.380[2]	4.204[–8]	4.193[1]	3.394[–7]	6.202[2]	4.011[–9]	1.297[1]	8.997[–8]	6.913[1]
$n = 9$	1.991[–7]	3.864[2]	2.119[–8]	7.292[1]	4.391[–8]	1.383[2]	2.246[–7]	6.712[2]	1.808[–7]	1.008[2]				
$n = 10$	3.614[–8]	3.012[2]	1.807[–7]	1.345[2]	1.167[–7]	7.492[2]	1.595[–7]	4.813[2]	2.179[–8]	1.112[2]				
$n = 11$	2.204[–8]	1.996[2]	8.141[–8]	1.518[2]	8.165[–8]	1.518[2]	1.169[–7]	4.538[2]	1.087[–7]	7.399[2]				
$n = 12$	7.403[–8]	7.725[2]	6.715[–8]	1.742[2]	9.313[–8]	4.912[2]	9.120[–8]	1.677[2]	1.192[–8]	2.828[2]				
$n = 13$	6.594[–8]	7.657[2]	6.850[–8]	1.824[2]	1.199[–8]	2.194[2]	6.843[–8]	1.824[2]	6.918[–8]	4.769[2]				
$n = 14$	1.065[–7]	1.914[2]	3.424[–8]	2.069[2]	–5.017[–9]	2.028[2]	5.333[–8]	7.728[2]	5.467[–8]	4.822[2]				
$n = 15$	4.443[–8]	4.896[2]	4.295[–8]	7.807[–2]	6.033[–8]	1.975[2]								
$n = 16$	3.334[–8]	7.964[2]	8.406[–8]	2.080[2]	2.742[–8]	2.080[2]	5.103[–9]	2.527[2]	3.781[–8]	5.061[2]				
$n = 17$	2.970[–8]	2.234[2]	3.094[–8]	5.047[2]	3.881[–8]	2.115[2]	2.840[–8]	7.965[2]	3.958[–8]	2.115[2]				
$n = 18$	4.253[–8]	2.167[2]	1.861[–8]	2.306[2]	2.617[–8]	5.103[2]	3.970[–8]	2.167[2]	2.364[–8]	8.022[2]				

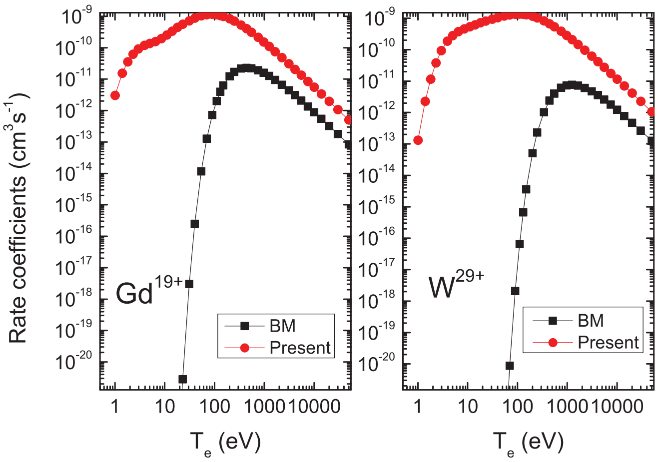

FIG. 9. (Color online) Comparison of present calculated DR rate coefficients with semiempirical BM approximation.

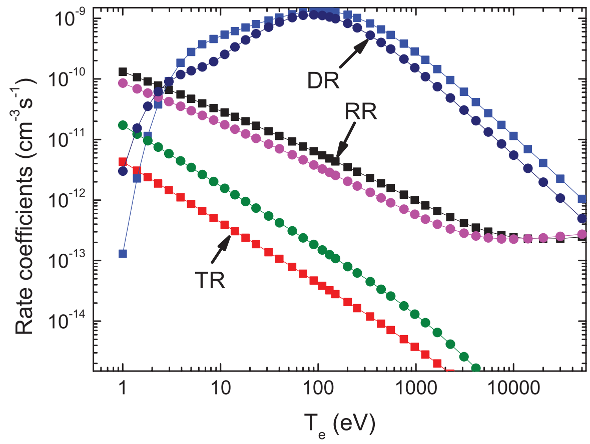

FIG. 10. (Color online) Comparison of the DR, TR, and RR rate coefficients for Rh-like Gd (circles) and W (squares). The TR rate coefficients calculated for electron density $n_e = 10^{20}$ cm^{-3} are presented.

present calculated DR rate coefficients with the predictions of the BM approximation in Fig. 9. Here we limited use to $4p$-$4d$ and $4d$-$4f$ transitions as suggested by Breton *et al.* [36]. The necessary atomic data were calculated using FAC. It is clearly seen from this figure that the BM approximation is totally incorrect at very low temperatures and, while it reproduces the overall trend very well, may underestimate the DR coefficients by up to a factor 2.2 for higher temperatures. The BM formula provides DR rate coefficients with an accuracy of about 60% for Gd and 40% for W when the temperature exceeds 40 eV. This result suggests that the BM formula provides a good estimate of the total DR rate coefficient for high-Z ions at temperatures higher than this value if scaled up by a factor close to two.

The calculated DR rate coefficients are fitted using following the semiempirical formula (in cm^{3}s^{-1}):

$$\alpha(kT_e) = kT_e^{-3/2} \sum_i c_i e^{(-\frac{E_i}{kT_e})}, \tag{7}$$

where c_i and E_i are the fitting coefficients. The fitting coefficients are given in Tables I and II. The differences between the fitted and the calculated data are less than 1% for temperatures above 15 eV. However, one should be careful to use the fitted data at temperature below 15 eV since the DR rates are very sensitive to resonance energies in that region.

The three-body (TR) and radiative recombination (RR) rate coefficients were calculated using empirical formulae [37] and are presented in Fig. 10 to show the influence of different recombination mechnisms for plasma balance modeling. For Gd, recent calculations predict that the optimum plasma temperature for EUVL source operation is close to 110 eV which gives maximum brightness at 6.76 nm. The DR rate coefficient reaches a maximum between 30 and 130 eV for Gd. For W, a collisional-radiative model calculation [37] predicts that the $4d$ open shell ions (W^{28+}–W^{37+}) are the dominant ionic species produced in the 200–800 eV region. The ionic population of Rh-like W (W^{29+}) reaches a maximum near 300 eV. It is clearly seen from Fig. 9 that the DR rate coefficient is about two orders of magnitude greater than the RR rate coefficient. There is thus no doubt that the DR process can have an important influence on plasma ionic population calculations. However, the DR process is ignored in many collision-radiative models due to lack of DR rate coefficient data. Further studies on how inclusion of the DR process changes the ion populations will be interesting and is urgently needed. For W, the DR process is the main power loss mechanism in fusion edge plasmas. A systemic study on other ions of W which can supply reliable data for the study of impurity transport processes and collisional-radiative modelling is required, especially in light of the importance of W containing plasmas for ITER and beyond.

IV. CONCLUSION

In this paper, level-by-level DR rate coefficients for Rh-like Gd and W based on FAC calculations have been presented. Since the energy levels become more tightly bound as Z increases, there are more doubly excited states below the ionization limit for W than Gd. The resulting closure of more AI channels means that the contribution of NRS becomes significantly greater and is already compareable with that from RS at temperatures higher than 25 eV for W. Comparison shows that the BM semiempirical formula significantly underestimates the DR rate coefficients at very low energies but if increased by a factor close to two provides a very good estimate at temperatures >40 eV. Because of their technological importance, *ab initio* calculations on other open $4d$ stages of both Gd and W are required. The rate coefficients calculated in the present work will be useful for modeling spectral emission both in hot plasmas for EUV lithography source development and fusion applications.

ACKNOWLEDGMENTS

We would like to acknowledge support from Science Foundation Ireland under Grant No. 07/IN.1/I1771. One of Authors (B.L.) would like to acknowledge financial support from a UCD-CSC scholarship award.

[1] M. H. Chen, Phys. Rev. A **35**, 4129 (1987).
[2] E. Behar, P. Mandelbaum, J. L. Schwob, A. Bar-Shalom, J. Oreg, and W. H. Goldstein, Phys. Rev. A **52**, 3770 (1995).
[3] E. Behar, P. Mandelbaum, J. L. Schwob, A. Bar-Shalom, J. Oreg, and W. H. Goldstein, Phys. Rev. A **54**, 3070 (1996).
[4] A. E. Kramida and T. Shirai, At. Data Nucl. Data Tables **95**, 305 (2009).
[5] A. E. Kramida and T. Shirai, At. Data Nucl. Data Tables **95**, 1051 (2009).
[6] A. Kramida, Can. J. Phys. **89**, 551 (2011).
[7] J. Reader, Phys. Scr. **T134**, 014023 (2009).
[8] J. Clementson, P. Beiersdorfer, G. V. Brown, M. F. Gu, H. Lundberg, Y. Podpaly, and E. Träbert, Can. J. Phys. **89**, 571 (2011).
[9] E. Behar, A. Peleg, R. Doron, P. Mandelbaum, and J. L. Schwob, J. Quant. Spectrosc. Radiat. Transfer **58**, 449 (1997).
[10] A. Peleg, E. Behar, P. Mandelbaum, and J. L. Schwob, Phys. Rev. A **57**, 3493 (1998).
[11] E. Behar, P. Mandelbaum, and J. L. Schwob, Phys. Rev. A **59**, 2787 (1999).
[12] E. Behar, P. Mandelbaum, and J. L. Schwob, Eur. Phys. J. D **7**, 157 (1999).
[13] F. C. Meng, C. Y. Chen, Y. S. Wang, and Y. M. Zou, J. Quant. Spectrosc. Radiat. Transfer **109**, 2000 (2008).
[14] F. C. Meng, L. Zhou, M. Huang, C. Y. Chen, Y. S. Wang, and Y. M. Zou, J. Phys. B **42**, 105203 (2009).
[15] C. Biedermann, R. Radtke, R. Seidel, and E. Behar, J. Phys: Conf. Ser. **163**, 012034 (2009).
[16] U. I. Safronova, A. S. Safronova, and P. Beiersdorfer, At. Data Nucl. Data Tables **95**, 751 (2009).
[17] U. I. Safronova, A. S. Safronova, and P. Beiersdorfer, J. Phys. B **42**, 165010 (2009).
[18] U. I. Safronova, A. S. Safronova, and W. R. Johnson, J. Phys. B **43**, 144001 (2010).
[19] U. I. Safronova, A. S. Safronova, P. Beiersdorfer, and W. R. Johnson, J. Phys. B **44**, 035005 (2011).
[20] U. I. Safronova, A. S. Safronova, and P. Beiersdorfer, Can. J. Phys. **89**, 581 (2011).
[21] U. I. Safronova, A. S. Safronova, and P. Beiersdorfer, J. Phys. B **45**, 085001 (2012).
[22] U. I. Safronova and A. S. Safronova, Phys. Rev. A **85**, 032507 (2012).
[23] S. Schippers, D. Bernhardt, A. Müller, C. Krantz, M. Grieser, R. Repnow, A. Wolf, M. Lestinsky, M. Hahn, O. Novotny, and D. W. Savin, Phys. Rev. A **83**, 012711 (2011).
[24] C. P. Ballance, S. D. Loch, M. S. Pindzola, and D. C. Griffin, J. Phys. B **43**, 205201 (2010).
[25] J. Sugar, V. Kaufman, and W. L. Rowan, J. Opt. Soc. Am. B **10**, 1321 (1993).
[26] J. Sugar, V. Kaufman, and W. L. Rowan, J. Opt. Soc. Am. B **10**, 799 (1993).
[27] B. Li, A. Endo, T. Otsuka, C. O'Gorman, T. Cummins, T. Donnelly, D. Kilbane, W. Jiang, T. Higashiguchi, N. Yugami, P. Dunne, and G. O'Sullivan, Proc. SPIE **8139**, 81390P (2011).
[28] B. W. Li, P. Dunne, T. Higashiguchi, T. Otsuka, N. Yugami, W. H. Jiang, A. Endo, and G. O'Sullivan, Appl. Phys. Lett. **99**, 231502 (2011).
[29] B. W. Li, G. O'Sullivan, Y. B. Fu, and C. Z. Dong, Phys. Rev. A **85**, 012712 (2012).
[30] M. F. Gu, Astrophys. J. **590**, 1131 (2003).
[31] E. Behar, P. Mandelbaum, J. L. Schwob, A. Bar-Shalom, J. Oreg, and W. H. Goldstein, Phys. Rev. A **52**, 3770 (1995).
[32] A. E. Kramida and J. Reader, At. Data Nucl. Data Tables **92**, 457 (2006).
[33] Y. B. Fu, C. Z. Dong, M. G. Su, F. Koike, G. O'Sullivan, and J. G. Wang, Phys. Rev. A **83**, 062708 (2011).
[34] A. Burgess, Astrophys. J **141**, 1588 (1965).
[35] A. Merts, R. D. Cowan, N. H. J. Magee, Los Almos Scientific Laboratory Report No. LA-6220-MS, 1976 (unpublished).
[36] C. Breton, C. De Michelis, and M. Mattioli, J. Quant. Spectrosc. Radiat. Transfer **19**, 367 (1978).
[37] D. G. Colombant and D. F. Tonon, J. Appl. Phys. **44**, 3524 (1973).